Anomalous *F* region response to moderate solar flares

C. G. Smithtro,[1] J. J. Sojka,[2] T. Berkey,[3] D. Thompson,[2] and R. W. Schunk[2]

Received 26 August 2005; revised 8 January 2006; accepted 24 February 2006; published 1 June 2006.

[1] Ionograms recorded with a dynasonde at Bear Lake Observatory, Utah, during moderate solar x-ray flares exhibit characteristic enhancements to the E and F_1 region ionosphere. However, during these same flares, the peak electron density of the ionosphere (N_mF_2) unexpectedly decreases, recovering after the flare ends. In order to reconcile this anomalous behavior with expected increases to the total electron content (TEC), we undertake a modeling effort using the Time-Dependent Ionospheric Model (TDIM) developed at Utah State University. For solar input, a simple flare time irradiance model is created, using measurements from the Solar EUV Experiment instrument on the TIMED spacecraft. TDIM simulations show that the anomalous N_mF_2 response can be explained by assuming a rapid electron temperature increase, which increases the O^+ scale height, moving plasma to higher altitudes. The model results are able to reproduce both the decreasing N_mF_2 as well as the expected TEC enhancement.

Citation: Smithtro, C. G., J. J. Sojka, T. Berkey, D. Thompson, and R. W. Schunk (2006), Anomalous *F* region response to moderate solar flares, *Radio Sci.*, *41*, RS5S03, doi:10.1029/2005RS003350.

1. Introduction

[2] Past and present study of the ionospheric response to solar x-ray flares has focused almost exclusively on the largest-magnitude events. Most of the early papers that described changes within the *F* region ionosphere focused on flares with optical 2B or 3B importance using incoherent scatter radars (ISRs) [*Thome and Wagner*, 1971; *Mendillo and Evans*, 1974]. More recently, the emphasis has shifted to using the total electron content (TEC), inferred from the Global Positioning System (GPS) signals, to describe the net ionospheric response [e.g., *Zhang et al.*, 2002]; however, the largest flares, such as the Bastille Day flare of 2000 or "Halloween" storms of 2003, still garner the most attention [e.g., *Dymond et al.*, 2004; *Tsurutani et al.*, 2005; *Huba et al.*, 2005].

[3] In this paper we examine ionospheric measurements made with the dynasonde at Bear Lake Observatory, during 10 moderate solar flares, focusing primarily on one case study example. While expected flare time enhancements are found in the E and F_1 regions, the electron density at the F_2 region peak exhibits an anomalous decrease. We are able to simulate this behavior using a modified ionospheric model and find that the decrease can be explained by enhanced electron gas temperatures, which change the scale heights, moving plasma to higher altitudes.

2. Ionospheric Observations at Bear Lake Observatory

[4] Utah State University operates a dynasonde at Bear Lake Observatory as part of a suite of instruments (data available at http://www.ngdc.noaa.gov/stp/IONO/Dynasonde/). The dynasonde provides high-resolution, middle-latitude (49.7° magnetic) ionospheric measurements at a 5-min cadence with an excellent signal-to-noise ratio. The ionograms it produces are ideal for studying the altitude-dependent ionospheric flare response, as long as the flare is not so large that enhanced *D* region absorption blocks the entire signal. This restricts our study to moderate solar x-ray flares, typically X1 class or smaller (i.e., GOES 0.1–0.8 nm flux less than $\sim 10^{-4}$ W/m^2). Figure 1 provides a representative picture of daytime ionograms taken with the dynasonde at Bear Lake Observatory. The data are plotted as a function of virtual height and frequency. In Figure 1, two ionograms are shown for comparison, both made near local noon on 22 June 1999. The first indicates ionospheric conditions at 1700 UT, prior to the onset of a solar x-ray flare, which began at 1815 UT. The second

[1]Air Force Institute of Technology, Wright-Patterson Air Force Base, Ohio, USA.
[2]Center for Atmospheric and Space Sciences, Utah State University, Logan, Utah, USA.
[3]Physics Department, Utah State University, Logan, Utah, USA.

0048-6604/06/2005RS003350$11.00

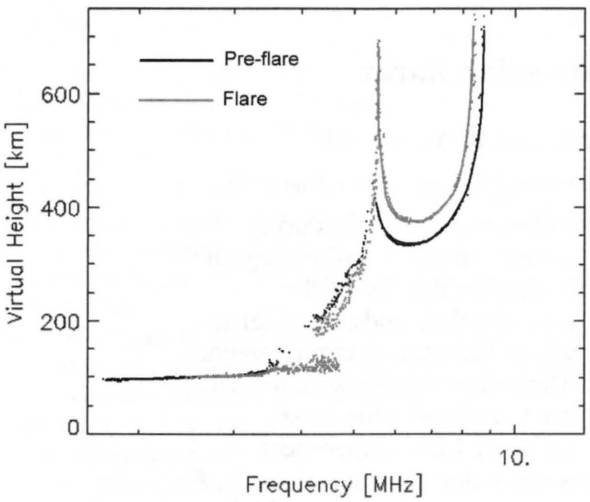

Figure 1. Two ionograms taken at the Bear Lake Observatory are plotted as a function of virtual height and frequency. The ionograms were taken prior to and during an M-class solar x-ray flare. See color version of this figure in the HTML.

ionogram depicts the conditions during the decay phase of the flare, measured at 1915 UT. In the diagram, asymptotes or cusps in the virtual height at a specific frequency identify critical ionospheric frequencies, such as f_oF_1 and f_oF_2; for clarity we have shown only those data corresponding to the ordinary mode. For example, in Figure 1, f_oF_2 falls between 8 and 9 MHz. There is also a well-developed peak in the F_1 region, as evidenced by the f_oF_1 strong cusps between 5 and 6 MHz. The signal in the lower E region is fairly noisy, and it is difficult to visually identify an f_oE asymptote; however, the E region is significantly enhanced between the two measurements. Given that the critical frequency goes as the square root of the electron density, this represents the expected electron density increase accompanying the flare.

[5] In the F_1 region we also see a small enhancement of electron densities over the course of the flare. The asymptote corresponding to f_oF_1 shifts slightly to the right. However, at the F_2 peak, the situation is reversed. On the basis of Figure 1, f_oF_2 decreases during the flare, indicating a commensurate decrease in the electron density at this altitude (N_mF_2). This runs counter to our intuitive expectation that increased solar flux during the

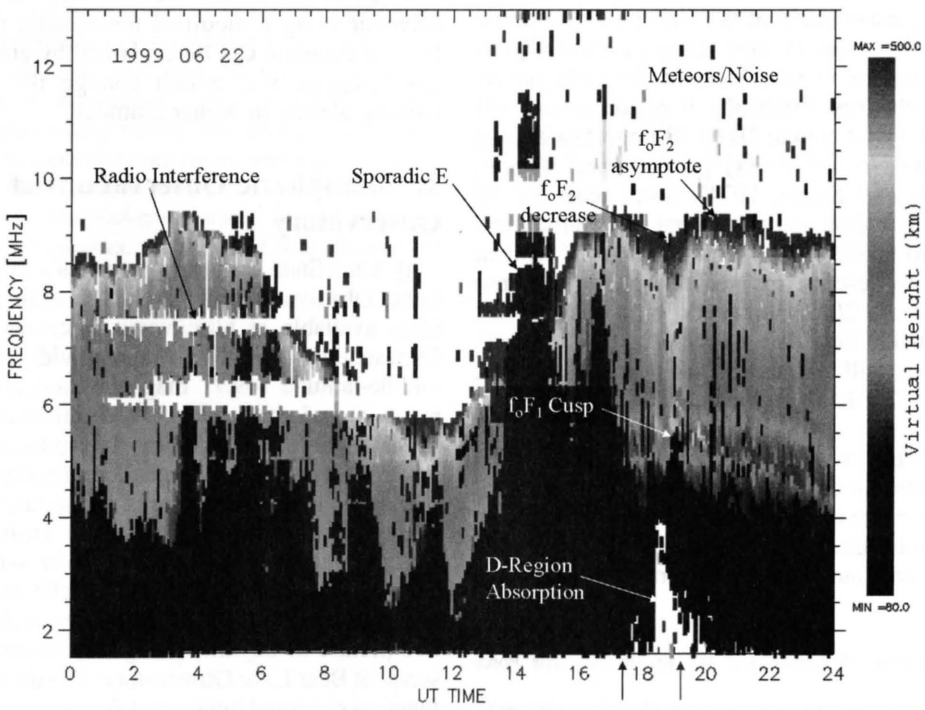

Figure 2. Full 24 hours of ionograms taken at 5 min cadence from the Bear Lake Observatory on 22 June 1999. The ionogram is plotted as a function of signal frequency and UT time; the shading represents the virtual height of the returned signal. Important features in the figure are identified and discussed further in the text. See color version of this figure in the HTML.

flare should lead to enhanced electron densities. Although most of the flux enhancement occurs in the x-ray wavelengths, affecting the lower *D* and *E* region ionosphere, we might expect at least a small increase in the flux at longer wavelengths. Even assuming no change in the EUV photon flux, it is initially difficult to understand why f_oF_2 would decrease during the flare.

[6] A better view of the temporal change is possible by examining many sequential ionograms taken throughout the duration of the flare and subsequent recovery. Figure 2 depicts such a series of measurements covering the full 24 hours of 22 June 1999. Ionograms are not typically presented in such a manner but are quite useful once the reader is accustomed to interpreting them. They are plotted with the signal frequency along the *y* axis and UT hour on the *x* axis. The virtual height of the returned signal is color coded or gray scaled. Virtual heights above 500 km are shown as white, so the f_oF_2 asymptote is indicated by the sudden transition to white at the higher frequencies. By tracking this transition over the course of the day, one observes the diurnal f_oF_2 variation: starting at ~8.5 MHz at 0000 UT, dropping to ~6 MHz near 1200 UT, and rising again to 9–9.5 MHz with local daylight hours.

[7] Local maxima in the *E* and F_1 regions, which produce asymptotes or cusps in the standard ionogram, appear as inversions of the virtual height in a full-day plot. In Figure 2 we are able to identify an inversion near 5 MHz and between 1700 and 2400 UT that corresponds to the *E* region peak. The frequency of this inversion exhibits a characteristic shape, corresponding to the change of solar zenith angle over the course of the day. For most of the day, there is not a local F_1 maximum and hence no strong F_1 inversion; however, during the flare, the F_1 region is enhanced, and a height inversion is observed corresponding to the f_oF_1 cusp identified in Figure 1.

[8] White horizontal cutouts in Figure 2 correspond to persistent radio interference at specific frequencies. Sporadic *E* is also a problem at this time of year over Bear Lake. The occurrence of sporadic *E* is indicated by the very dark returns extending from the bottom of the plot up to higher frequencies and at all UT times. The dark shading corresponds to a low virtual height, indicative of the *E* region. In Figure 2, sporadic *E* masks the f_oE inversion between 1200 and 1700 UT.

[9] The fact that an M1 x-ray flare occurs at ~1900 UT is immediately apparent from the full-day ionogram. At the bottom of Figure 2, there is a cutout in the data between roughly 1800 and 2000 UT. This cutout appears white in the data because no signal returned to the dynasonde, corresponding to absorption in the *D* region ionosphere. The shape of the cutout correlates well with the 0.1–0.8 nm x-ray flux measured by the GOES spacecraft. Two small vertical arrows on the *x* axis indicate the respective times (1700 and 1915 UT) of the ionograms shown previously in Figure 1. The anomalous decrease in f_oF_2, described earlier in Figure 1, now appears as a notch in the f_oF_2 asymptote. On the basis of this single event, the f_oF_2 "flare notch" appears to occur on roughly the same timescale as the solar x-ray flare.

[10] A preliminary investigation of the available data over the period 1999–2001 revealed a total of 10 "clean" x-ray flare events, all of which exhibited some form of f_oF_2 "flare notch." During this period, more than 10 x-ray flares occurred, but not every flare produced an observable effect in the ionosphere over Bear Lake. For this investigation, ionospheric flare events were identified by visually searching the dynasonde database for *D* region absorption cutouts (as depicted in Figure 2). Candidate flares therefore needed to be strong enough to induce an obvious *D* region cutout, but not so strong as to cause absorption of the entire signal. This eliminated most flares larger than X1 class and smaller than M1; flares also had to occur near local noon. Noise associated with sporadic *E* marred much of the summertime data, while other days were eliminated because of strong geomagnetic activity or multiple flares over a relatively short period. These criteria reduced the number of usable flare events to 10. Of these, all 10 exhibited the expected increases in f_oE and f_oF_1, as well as anomalous decreases in f_oF_2 corresponding to F_2 region electron density depletions of ~10%.

3. Ionospheric Model

[11] For this work we modeled the ionosphere using the Time-Dependent Ionospheric Model (TDIM) developed at Utah State University. In the TDIM, the continuity, momentum, and energy equations are solved using a Lagrangian formulation for a magnetic flux tube, including all relevant *E* and *F* region processes. The flux tube drifts in response to an imposed electric field convection pattern specified by the *Kp* index; however, for the latitude and geomagnetic conditions considered in this paper, the drift effectively reduces to corotation with the Earth. The ion and electron temperatures are rigorously calculated at all altitudes, using a parameterization of the electron volume heating rate based on the 10.7 cm radio flux ($F_{10.7}$). *Schunk* [1988] gives a detailed review of the TDIM theoretical development, while comparisons with observations are discussed by *Sojka* [1989]. Although heating rates certainly increase during solar flares, we assume that the neutral atmosphere remains unaffected over the relatively short timescales considered here and specify it using the Mass Spectrometer Incoherent Scatter empirical model [*Hedin*, 1991].

[12] As an input to the TDIM, the flux of EUV photons (5–105 nm) is specified by the EUV for Aeronomic Calculations (EUVAC) model [*Richards et al.*, 1994],

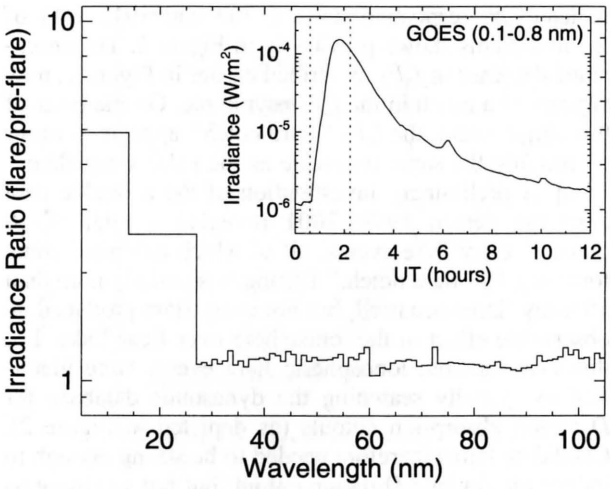

Figure 3. Ratio of the measured flare irradiance to the preflare irradiance as a function of wavelength. The two measurements were made by the SEE instrument on the TIMED satellite at 0036 and 0214 UT [*Woods et al.*, 2003] on 21 April 2002. The GOES x-ray flux during this period is also shown (inset); dotted lines correspond to the times of the respective SEE measurements.

which uses the daily 10.7 cm radio flux ($F_{10.7}$) and its 81-day centered average ($\langle F_{10.7} \rangle$) as proxies. The EUVAC model specifies the solar irradiance in 37 wavelength bins to represent a combination of important emission lines and broad bands. *Richards et al.* [1994] also provide intensity-weighted absorption and ionization cross sections for use in conjunction with the EUVAC model. However, the EUVAC irradiance model provides no inherent capability to specify the irradiance during a solar flare. To do this, we relied on recent measurements made by the Solar EUV Experiment (SEE) on the TIMED satellite (data level 3A, calibration version 8).

[13] The SEE instrument on TIMED was designed to measure the spectral irradiance between 0.1 and 195 nm [*Woods et al.*, 1998]. Its observations of the Sun are limited to roughly one 3-min interval per 97-min orbit [*Woods et al.*, 2003] and are thus not ideally designed to study solar flares. However, as reported by *Woods et al.* [2003], the SEE science team has managed to capture a number of solar flares. On 21 April 2002, a solar x-ray flare occurred, reaching a maximum category of X1 at approximately 0150 UT. Prior to flare onset, the SEE instrument made an irradiance measurement at 0036 UT, when the x-ray flux level was at roughly C7 levels. Another measurement followed just after the peak of the flare at 0214 UT, while the x-ray flux was still near X1 levels.

[14] The ratio of these two irradiance spectra is shown in Figure 3 as a function of wavelength. An inset in Figure 3 details the GOES x-ray flux (0.1–0.8 nm) during this particular flare; dotted lines indicate the times of the corresponding EUV measurements by the SEE instrument. As expected, the majority of the irradiance increase is found at the shortest wavelengths; between 5 and 14 nm, the energy flux increases by nearly a factor of 5. From 14 to 27 nm, the flux increases by a factor of 2.6. At longer wavelengths, the ratio approaches unity; a logarithmic scale is used to accentuate these smaller changes. While the absolute measurements made by SEE are only applicable to this specific flare, we can use the ratios shown in Figure 3 to create a simple flare time irradiance model that can then be applied to other flares. Flare spectra are highly variable and unique; thus, for any given flare, these ratios provide only a crude approximation to the actual irradiance increase. In general, lower-intensity flares have softer spectra, and applying X1-flare ratios to M1 class events is not ideal, but in lieu of measurements or a true flare time model provides a reasonable first-order approximation.

[15] The flare time irradiance model is a simple addition to the standard EUVAC model. The irradiance increases measured by SEE for the 21 April 2002 X1 flare are assumed to apply generally to moderate x-ray flares. As a coarse approximation of the ratios presented in Figure 3, we assume that at its peak, an X1 class flare increases the photon flux between 5 and 15 nm by a factor of 5, and by a factor of 2.6 between 15 and 25 nm. All other wavelengths are assumed to be unaffected. In order to represent smaller M-class flares, the relative increase in each wavelength bin is scaled downward linearly, based on the magnitude of the flare in question. The temporal variation of these scale factors is determined by using the GOES soft x-ray flux as a proxy. Over the flare period, the GOES data are fit using a lognormal function, which then provides an analytic expression to compute the scale factors as a function of time. Within the ionospheric model, EUVAC is used to represent the background Sun, based on $F_{10.7}$ and $\langle F_{10.7} \rangle$. Once the simulation time reaches the beginning of the flare event, the lognormal function is used to drive the behavior of the flare scaling factors, which are applied to the background EUVAC irradiance.

[16] The main focus of this paper is the M1 x-ray flare that occurred on 22 June 1999. Figure 4 details the evolution of this flare, as well as the performance of the simple flare time irradiance model. The top plot of Figure 4 presents the GOES x-ray flux (0.1–0.8 nm) between 1200 and 2400 UT. The x-ray flare began at approximately 1815 UT and reached a maximum flux of 1.8×10^{-5} W/m^2 (M1.8) at 1830 UT. Simultaneous measurement of the EUV photon flux is available from the Solar EUV Monitor (SEM) on the SOHO satellite

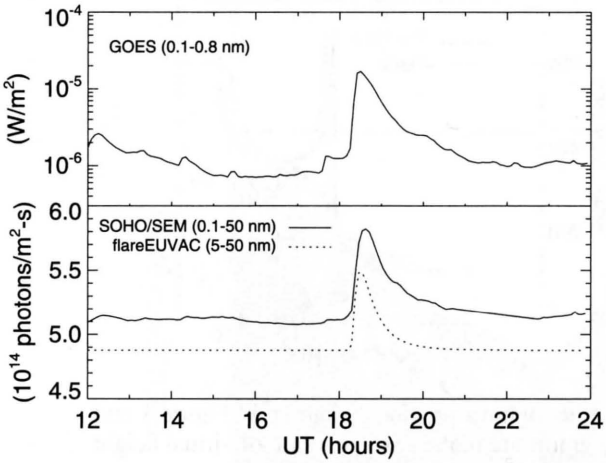

Figure 4. (top) GOES x-ray energy flux and (bottom) SOHO/SEM integrated (0.1–50 nm) EUV photon flux as a function of time over the course of an M1 x-ray flare on 22 June 1999. A dotted line depicts the behavior of the modified flare-time EUVAC model, described in the text, integrated over 5–50 nm.

[*Judge*, 1998]. The bottom plot of Figure 4 details the integrated 0.1–50 nm photon flux measured by SEM. The standard SEM data products contain the measured irradiance in two bands, a narrow 26–34 nm band and broad 0.1–50 nm band. We display the broad band since it includes shorter wavelengths most subject to flare increase. In our simple flare model, wavelengths greater than 25 nm are assumed constant, and indeed, SEM registered only a 4% increase in the narrow 26–34 nm band (not shown) during the 22 June 1999 flare.

[17] Prior to flare onset, the SEM instrument measured an integrated (0.1–50 nm) photon flux of 5.1×10^{14} m^{-2} s^{-1}. At the peak of the flare (1830 UT), the photon flux rose nearly 15% to 5.8×10^{14} m^{-2} s^{-1}. For comparison, the integrated photon flux predicted using the modified EUVAC model is also shown. On this day, $F_{10.7}$ and $\langle F_{10.7} \rangle$ were 167 and 165, respectively. Using these values, the standard EUVAC model generates an integrated (5–50 nm) photon flux of 4.9×10^{14} m^{-2} s^{-1}, 4% less than the preflare SEM measurement. Inclusion of additional photons in the range 0.1–5 nm is not enough to make up this difference. The Vacuum Ultra-Violet (VUV) irradiance model [*Woods and Rottman*, 2002], which extends to shorter wavelengths than EUVAC, suggests that under these conditions, photons in the range 0.1–5 nm only add $\sim 2 \times 10^{12}$ m^{-2} s^{-1}, or 0.5%, to the total integrated flux—not enough to bring EUVAC in line with the SEM measurement. However, our interest is not to exactly match the baseline conditions but rather to investigate the relative variation of the flux during the flare, and therefore we make no further attempt to reduce the offset.

[18] It is apparent from Figure 4 that the modified EUVAC model recreates both the shape and relative magnitude of the SEM response. Prior to the flare, the SEM and EUVAC fluxes differ by ~4%. Near the flare peak, the difference increases to 8%; however, if we again account for wavelengths less than 5 nm by appropriately scaling the VUV model, the difference drops to 6%. On this particular day, our simple flare time irradiance model is able to recreate the observed increase in photon flux. This comparison alone does not validate the spectral weighting of the simple flare model, since the quantities are integrated; however, given the weak response of the measured SEM 26–34 nm flux (+4%), our decision to hold wavelengths greater than 25 nm constant appears reasonable.

[19] The biggest limitation of the current modeling effort is that the TDIM does not self-consistently include the effect of photoelectrons. Photoelectrons are responsible for two important effects. The first is secondary ionization caused as the energetic photoelectrons collide with the neutral gas. The second is heating of ambient thermal electrons via Coulomb collisions. Under most conditions, these effects are reasonably approximated using simple empirical expressions. *Richards and Torr* [1988] showed that the additional ionization caused by photoelectrons can be approximated by applying a simple altitude- and species-dependent scale factor to the photoionization rates. This is the method currently employed in the TDIM. During a flare, additional photon flux at the short wavelengths increases the photoionization rate, which is reflected through the scale factors; however, the initial *Richards and Torr* [1988] work assumed a standard solar irradiance, and it is unclear how much the results change given a harder flare spectrum.

[20] To calculate the volume heating rate of the ambient electrons by photoelectrons, the TDIM currently uses a parameterized fit to the results of a generic photoelectron transport calculation. This simple parameterization depends solely on the solar zenith angle and $F_{10.7}$ radio flux and therefore does not reflect changes occurring during a flare. In order to more realistically represent the electron temperature during a solar flare, we apply a flare time increase to the volume heating rate. To do this, we recognized that the integrated EUV (5–105 nm) energy flux measured by the SEE instrument increased by a factor of 2.1 during the X1 flare depicted in Figure 3. For comparison, the integrated EUV energy flux increases by roughly a factor of 3 from solar minimum to maximum. We therefore calculate the ratio of the solar maximum to minimum electron volume heating rates and apply the altitude-dependent result as a scale factor to approximate the change induced by an X1 flare. Just as was done

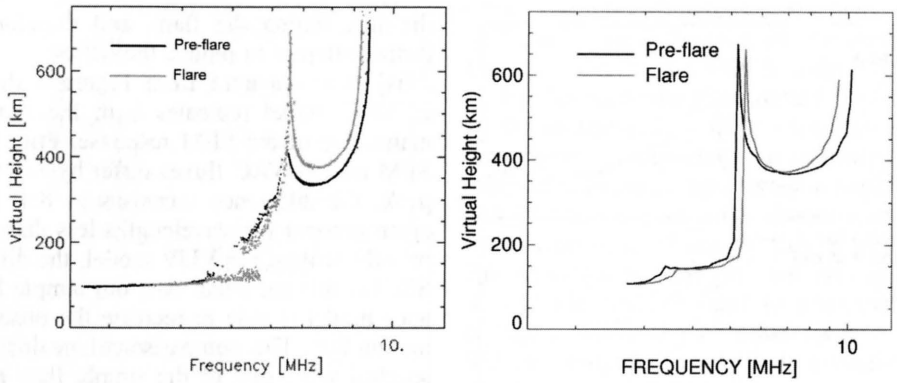

Figure 5. Comparison between (left) the measured ionograms previously shown in Figure 1 and (right) simulations created using the TDIM. All ionograms are plotted as a function of virtual height and frequency. See color version of this figure in the HTML.

previously, a lognormal fit to the GOES x-ray flux is used as a proxy to drive changes in the volume heating rate over the course of the flare. It is important to reiterate that the flare time increase applied to the electron heating rate was not based on any physical calculation; rather, it represents a coarse approximation, best justified by how well the model results compare with observations.

4. Model Results

[21] Using the TDIM and the flare time modifications described previously, we simulated the ionospheric effect of the M1 x-ray flare on 22 June 1999 in order to compare with the Bear Lake observations described above. Although it is possible to convert the measured ionograms into equivalent electron density profiles, the process requires a number of additional assumptions. It is more straightforward to instead turn the model output into a virtual ionogram using a ray-tracing algorithm such as that described by *Coleman* [1998]. This allows direct comparison of the simulated ionosphere with that measured by the dynasonde.

[22] In Figure 5, we present a comparison of the measured and simulated ionograms. The right plot of Figure 5 depicts virtual ionograms created from TDIM output using the *Coleman* [1998] routine. The plot contains two ionograms; one corresponds to ionospheric conditions prior to flare onset, valid at 1700 UT. The other corresponds to conditions after the peak of the flare, valid at 1915 UT. These are the same times as were described previously. For comparison, the left plot repeats the observations shown previously in Figure 1.

[23] While comparing Figures 1 and 5, we immediately see differences between the measured and simulated ionosphere. Overall, the modeled f_oF_2 is too high, and there are qualitative differences between the transition from E to F_1 and F_1 to F_2 regions. Although there are some fairly significant differences between the observations and simulations, these relate more to the calibration of the TDIM to the baseline conditions rather than the flare time dynamics. In fact, the model was able to capture the flare-specific trends described previously. At the times shown, the simulation has recreated the expected increase in f_oE and f_oF_1, as well as the anomalous f_oF_2 decrease. Quantitative differences between the observed and simulated flare response are likely due to our simple treatment of the irradiance and photoelectron effects; additional work is planned to address these deficiencies.

[24] Figure 6 represents a simulation of the full-day ionogram, equivalent to measured data shown in Figure 3. The simulated ionogram obviously lacks the sporadic E and radio interference found in Figure 3 and does not account for D region absorption but otherwise strongly resembles the observations. Because of the baseline differences between the observed and modeled ionogram described above, the shading of Figures 3 and 6 differs; however, the flare-induced changes are immediately apparent and similar, particularly in f_oF_2.

[25] During the daylight hours, inversions of the virtual height between 4 and 6 MHz represent the E and F_1 regions. Superimposed upon this is the flare enhancement, which follows a temporal response dictated by the GOES x-ray flux proxy, increasing rapidly at 1815 UT and reaching a maximum at 1830 UT. At the F_2 peak, we are able to recreate the shape of the flare notch described previously. The magnitude and duration of the notch can be quantified by the difference in f_oF_2 computed from two simulations, one including flare effects and the other without. Unlike the E and F_1 response, the phase of the f_oF_2 depression does not simply mirror the GOES x-ray

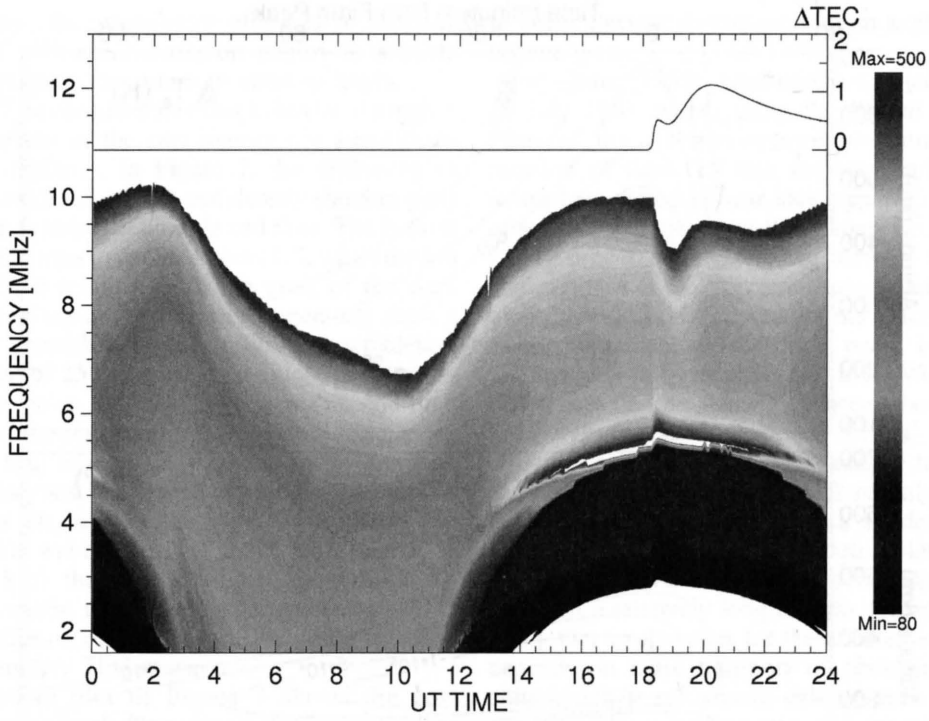

Figure 6. Simulation of ionograms valid on 22 June 1999 over the Bear Lake Observatory. The ionogram is plotted in the same manner as Figure 2. A solid line and secondary *y* axis correspond to the increase of TEC (10^{16} electrons/m^2) between the flare and nonflare simulations. See color version of this figure in the HTML.

proxy. The notch begins to form within two model time steps of flare onset, 10 min, but does not reach its absolute maximum difference (0.75 MHz) until 20 min after the peak of the flare. It takes another hour for f_oF_2 to recover (80 min after the peak of the flare). The physical significance of these results is discussed further below.

[26] At the top of Figure 6, a solid line corresponds to the increase in total electron content (TEC) between the flare simulation and one that neglected flare effects. It is given in standard TEC units (1 TEC unit = 10^{16} electrons/m^2) on a secondary *y* axis. Even as f_oF_2 decreases, we still recover the expected flare time TEC increase. Many previous studies have demonstrated TEC enhancements during solar flares [e.g., *Zhang et al.*, 2002], and it is reassuring to reproduce this effect. The simulated flare time TEC increase displays an interesting double peak structure. The initial peak corresponds to an increase of 0.5 TEC units above the nonflare simulation and occurs simultaneous to the x-ray flare maximum (1830 UT). This initial response is obviously driven by the enhanced short wavelength photons in the irradiance model (per Figure 3), which cause additional ionization, primarily in the *E* and lower F_1 regions. However, at this point, f_oF_2 has already started to decrease, and the question remains how to reconcile a TEC increase with a simultaneous decrease of N_mF_2.

[27] After the peak of the flare, the irradiance enhancement begins to decrease and initially, so does TEC; however, 20 min after the peak of the flare, TEC begins to increase again, reaching a second local maximum 105 min after the flare peak, roughly 1 TEC unit above the background. This second TEC enhancement is certainly not caused by direct ionization; by this time, the irradiance has returned to near-background levels (Figure 4). As we will see, the behavior of f_oF_2 and TEC can both be explained by an increase in the plasma temperature.

[28] The bulk of TEC comes from the F_2 layer and is frequently approximated as the peak F_2 electron density (N_mF_2) multiplied by an equivalent *F* layer slab thickness. Given a low-altitude electron density enhancement, TEC should increase as long as the topside contribution remains roughly constant. The topside contribution to TEC can be approximated as $\mathrm{TEC}_{\mathrm{topside}} \approx N_mF_2 \times H_p$, where H_p is the plasma scale height at the F_2 peak. Since H_p goes as the plasma temperature, it is possible for the topside TEC to remain constant if the plasma temperature increases as N_mF_2 decreases. In fact, if topside TEC is assumed constant, then N_mF_2 and plasma temperature are inversely related. Enhanced plasma temperatures can

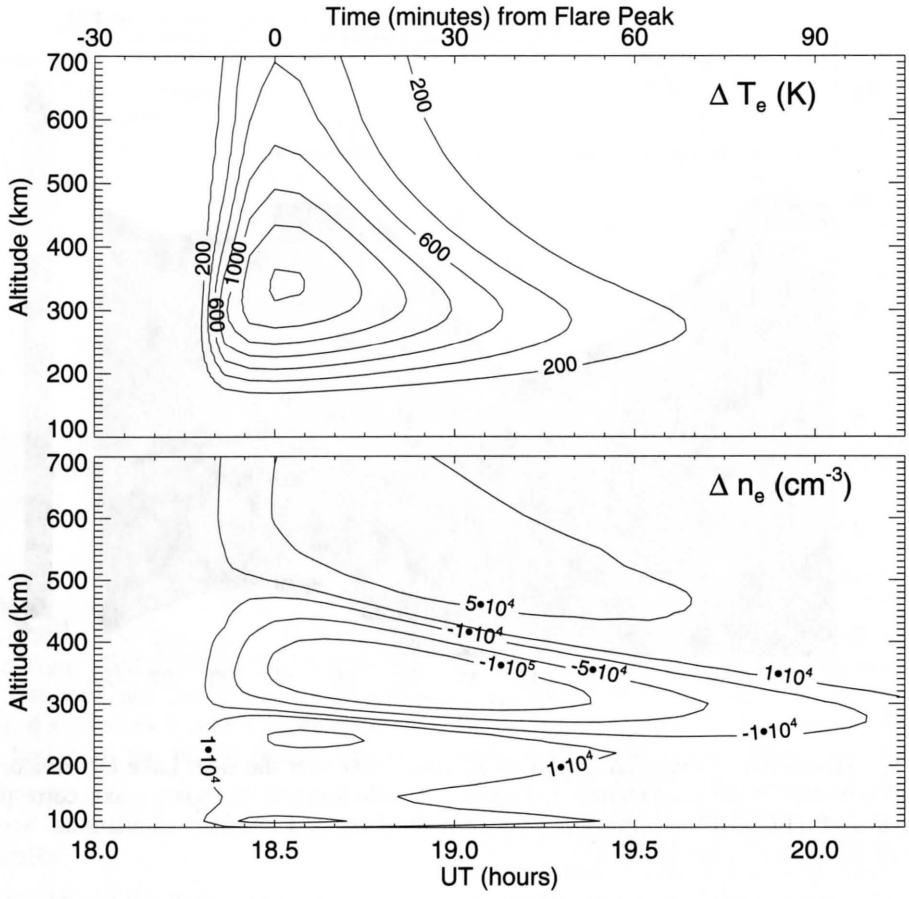

Figure 7. Differences in (top) the electron temperature and (bottom) density computed by two simulations; one included flare effects and the other did not, valid 22 June 1999 over the Bear Lake Observatory. The differences are plotted as a function of altitude and time in UT hours along the bottom x axis and minutes from the flare peak across the top; x axis ticks are spaced in 5-min increments. See color version of this figure in the HTML.

therefore reconcile the anomalous f_oF_2 flare notch and simultaneous increase to TEC. As we will see, enhanced temperatures are also the root cause of the f_oF_2 depression and secondary TEC maximum.

[29] Although most of the additional short-wavelength flare photons are deposited in the lower ionosphere, they produce copious photoelectrons which are then able to rapidly diffuse along magnetic field lines to all altitudes. Along this route, the photons deposit their energy into the thermal electron gas, increasing the electron volume heating rate and hence the plasma temperature. A rapid increase in temperature alters the plasma scale height, expanding the F_2 region and forcing diffusion to higher altitudes. In the case of the 22 June 1999 flare, the irradiance increases do not significantly increase production at the F_2 peak; continuity therefore requires f_oF_2 to decrease as the plasma shifts to higher altitudes, hence the depression of f_oF_2. In addition, the total topside electron content is conserved, so the initial TEC increase indicated in Figure 6 represents a direct flare enhancement of the E and F_1 region electron density. The second TEC maximum also depends on the temperature enhancement. As the F_2 region expands, the plasma moves to higher altitudes where the time constant for loss is much longer. The action of the flare time temperature enhancement is thus analogous to meridional neutral winds that frequently maintain the F layer after sunset. An equivalent increase in neutral temperature would negate much of this effect, since the neutral gas would also expand; however, given the relatively long time constant for changes in the neutral atmosphere, we assume it to be constant over the period in question. Enhanced electron temperatures therefore shift plasma to higher altitude over the duration of the flare notch; given

lower loss rates, the cumulative effect is to increase columnar TEC. This accumulation begins to subside after plasma temperatures return to nominal levels.

[30] Figure 7 better illustrates this behavior through a further comparison of the two ionospheric simulations (flare versus nonflare). In Figure 7, the difference in electron temperature (top plot) and density (bottom plot) are plotted as a function of altitude and time. The bottom x axis reports the time in decimal hours UT, while the top x axis gives it in minutes from the peak of the flare (1830 UT). Contours of the electron temperature show a rapid increase coincident to flare onset. The simulation used a step size of 250 s; at this resolution, the temperature increased up to 150 K (270 km) within one time step. Similarly, the maximum temperature difference of 1420 K (330 km) is effectively coincident to the peak of the flare. Beyond the peak, temperatures return to nominal levels on roughly the same timescale as the GOES x-ray flux and by 2015 UT are no more than 60 K higher (270 km) than the nonflare simulation. As described previously, these changes in temperature drive the upward diffusion of plasma responsible for the flare notch and secondary TEC maximum.

[31] The bottom plot of Figure 7 shows the corresponding change in electron density between the flare and nonflare simulations. In the lower E and F_1 regions, the enhanced photon flux increases the electron density directly via ionization. At the peak of the flare, the enhancement in this lower region reaches a maximum of 6×10^4 cm^{-3} at 110 km. As the flare strength decays, so does the density enhancement. Upward diffusion of the plasma is also apparent from Figure 7. Within 10 min of the flare onset, electron densities near the F_2 peak begin to decrease relative to the nonflare simulation; at the same time, topside densities are enhanced. As described previously, the maximum f_oF_2 depression occurs 20 min after the peak of the flare; this corresponds to an electron density decrease of 2×10^5 cm^{-3} at 350 km. At the same time, the topside ionosphere reflects upward diffusion with a peak increase of 7×10^4 cm^{-3} at 550 km.

5. Discussion

[32] Both observations and computer simulations suggest that during moderate solar flares, enhanced plasma temperatures can lead to a decrease of N_mF_2 as plasma diffuses to higher altitudes. This theory is bolstered by an analogous, yet opposite, effect reported 40 years ago. During investigations into the ionospheric response to solar eclipses, *Evans* [1965a, 1965b] reported anomalous increases in f_oF_2 at a number of locations commensurate with the eclipse. In a manner analogous to our discussion here, Evans invoked downward diffusion of plasma due to lower electron temperatures as an explanation for this enhancement.

[33] *Evans* [1965a] conducted a detailed analysis of the 20 July 1963 eclipse using the ISR at Millstone Hill. Plots of the electron temperature and density as a function of time (15 min cadence) indicated that the ionosphere varied in near lock step with the percentage of solar obscuration over the 1-hour rise to totality. This would suggest nearly zero lag between the obscuration and response of electron temperature and density. In our work, the electron temperature maximum is also effectively coincident to the flare peak, but the density minimum lags by roughly 20 min. We can reconcile differences in the density response both through the relatively coarse cadence of Evans' measurements (15 min) and the fact that the eclipse took a full hour to reach totality, whereas the flare only took 15 min. Flares hit the ionosphere with a sudden and dramatic temperature increase, and diffusion is slower to respond; an eclipse slowly decreases the temperature, allowing diffusion a relatively long time to keep pace.

[34] Our explanation for the anomalous f_oF_2 decrease depends on rapid transport of photoelectrons to high altitudes, their subsequent enhancement of the thermal electron volume heating rate, and resulting plasma temperature increase. Recent satellite measurements bear out this expectation. *Sharma et al.* [2004] examined the variation of electron and ion temperatures between flare and nonflare days using the Retarded Potential Analyzer onboard the Indian SROSS-C2 satellite; these measurements were made at altitudes between 425 and 625 km. Sharma et al. found that electron temperatures increased by a factor of 1.3 to 1.9 during flare events, while ion temperatures increased 1.2 to 1.4 times over nonflare days. Our simulation of the 22 June 1999 flare produced a comparable increase of 1.3 in the plasma temperature for similar altitudes at the flare maximum. Further comparison of satellite-based measurements with simulated temperatures would provide additional verification of our results.

[35] A literature search uncovered no previous references to the anomalous N_mF_2 decrease described in this paper; however, earlier work does provide some background for the conclusions presented here. The earliest flare time F region observations came using ISRs; *Thome and Wagner* [1971] present data from two optical 2B flares observed in 1967 over Arecibo. Their results demonstrated increased electron density below ~240 km but suggested a decrease throughout the topside ionosphere; this decrease began within minutes of the flare peak and continued throughout its duration. In their discussion, Thome and Wagner argued that this apparent negative fluctuation could be the result of inadequate plasma temperature information (required to correctly interpret the ISR measurements), electrodynamic effects

caused by flare-induced currents, or wave effects caused by traveling ionospheric disturbances. As Thome and Wagner make clear, their results are uncertain above 240 km, since they had to rely on estimates for the temperature correction. Given the measurement uncertainty, the Thome and Wagner results do not necessarily constitute a good comparison to our own.

[36] The work of *Mendillo and Evans* [1974] provides more compelling data; their ISR measurements were made over Millstone Hill during an optical 3B flare that occurred in 1972. Although their measurements of electron density do not exhibit an anomalous N_mF_2 decrease, they do show significant upward plasma drift during the flare. Prior to the flare, measured drifts were predominantly downward, but once the flare began, drifts above 375 km became upward. Mendillo and Evans conclude that this upward drift is associated with thermal expansion of the ionosphere driven by enhanced electron temperatures. The fact that Mendillo and Evans observed upward drifts but no anomalous N_mF_2 decrease could be due to the magnitude of the flare in question.

[37] Extreme events, such as the Bastille Day flare of 2000 and Halloween storms of 2003, are very different from the ones considered here. Specifically, the irradiance changes described for the X1 flare in Figure 3 no longer apply. On 28 October 2003, the TIMED/SEE instrument measured the irradiance changes during an X17 solar flare. In this extreme case, the irradiance at wavelengths between 5 and 14 nm increased by more than a factor of 20, by a factor of 1.2 between 14 and 27 nm, and by roughly a factor of 2 at longer EUV wavelengths up to 105 nm (T. N. Woods, private communication, 2005). No longer can we assume the majority of the EUV irradiance to be unaffected by the flare; the factor of 2 change across most of the EUV dramatically increases production rates in the F_2 region, possibly compensating for the thermal expansion described previously. The N_mF_2 decrease is likely a feature of more modest flares, for which the F_2 production rate remains relatively constant. Further modeling is planned to delineate the relative importance of thermal expansion versus increased photoionization over a range of flare strengths, but this will require an accurate, self-consistent calculation of the electron volume heating rate.

[38] We might also expect a latitudinal dependence to the N_mF_2 decrease. The TDIM is a midlatitude to high-latitude ionospheric model and is not accurate for latitudes much lower than those explored in this paper (49.7° magnetic), so we are currently unable to simulate the effect at low latitudes; however, the orientation of the magnetic field certainly plays an important role. The photoelectrons responsible for heating the thermal electron gas must be able to flow from low altitudes, where they are primarily created, to the F_2 region. Furthermore, once the plasma is heated, it must be able to diffuse vertically along the magnetic field. Both processes are dependent on the sine of the dip angle, and therefore we can expect the efficiency to go down as we move to lower magnetic latitudes. Returning to the solar eclipse analogy described above, *Evans* [1965b] found that the dip angle needed to be larger than 60° for the eclipse to cause a measurable effect. The same cutoff will likely not apply to the flare notch; however, the observations presented in this paper were made at Bear Lake Observatory, which has a local dip angle of approximately 67°.

6. Conclusions

[39] In the middle-latitude ionosphere, measured values of f_oF_2 unexpectedly decreased during moderate solar flares. Using ionograms measured at the Bear Lake Observatory near Logan, Utah, all 10 of the flares examined exhibited this behavior. After introducing flare time modifications to a standard ionospheric model, we were able to reproduce the observed f_oF_2 response and found that it could be explained in terms of thermal expansion caused by enhanced electron temperatures.

[40] Although we were able to simulate the observed ionospheric flare response, our modified model contained a number of limitations. Most significant were the simplified treatments of the EUV irradiance and photoelectrons. The simple EUV irradiance model introduced here was based on a single X1 solar x-ray flare measured by the SEE instrument on the TIMED satellite [*Woods et al.*, 2003]. Since that time, enough flares have been captured that a more sophisticated flare time irradiance model has been developed (P. Chamberlin, private communication, 2005). Future, expanded modeling efforts will make use of these results in order to more accurately examine a wide range of flare magnitudes.

[41] The next step in the modeling effort must also self-consistently treat photoelectrons in order to accurately account for increases in the thermal electron volume heating rate and secondary ionization by photoelectrons. It is important to reiterate that the technique employed here relied on an arbitrary, albeit justified, increase to the volume heating rate. A self-consistent treatment is required in order to validate the resulting plasma temperatures, which are responsible for the entire effect. The current model also neglects an expected increase in the fraction of ionization caused by photoelectrons. Again, this can only be remedied through a self-consistent treatment of photoelectrons. A more complete survey of the observational record is also planned in order to expand the number of events and to develop a climatology of the flare time N_mF_2 decrease.

[42] **Acknowledgments.** Christopher Smithtro is supported by the Air Force Institute of Technology and a grant from AFOSR. This research was also supported by NASA grant

NAG5-8227 and NSF grant ATM-0000171 to Utah State University. The authors would like to thank Tom Woods for providing the TIMED/SEE irradiance data. The views expressed in this article are those of the authors and do not necessarily reflect the official policy or position of the Air Force, the Department of Defense, or the U.S. government.

References

Coleman, C. J. (1998), A ray tracing formulation and its application to some problems in over-the-horizon radar, *Radio Sci.*, *33*(4), 1187–1198.

Dymond, K. F., S. A. Budzien, A. C. Nicholas, S. E. Thonnard, R. P. McCoy, R. J. Thomas, J. D. Huba, and G. Joyce (2004), Ionospheric response to the solar flare of 14 July 2000, *Radio Sci.*, *39*, RS1S25, doi:10.1029/2002RS002842.

Evans, J. V. (1965a), An *F* region eclipse, *J. Geophys. Res.*, *70*, 131–142.

Evans, J. V. (1965b), On the behavior of f_oF_2 during solar eclipses, *J. Geophys. Res.*, *70*, 733–738.

Hedin, A. E. (1991), Extension of the MSIS thermosphere model into the middle and lower atmosphere, *J. Geophys. Res.*, *96*, 1159–1172.

Huba, J. D., H. P. Warren, G. Joyce, X. Pi, B. Iijima, and C. Coker (2005), Global response of the low-latitude to midlatitude ionosphere due to the Bastille Day flare, *Geophys. Res. Lett.*, *32*, L15103, doi:10.1029/2005GL023291.

Judge, D. L. (1998), First solar EUV irradiance obtained from SOHO by the CELIAS/SEM, *Sol. Phys.*, *177*, 161–173.

Mendillo, M., and J. V. Evans (1974), Incoherent scatter observations of the ionospheric response to a large solar flare, *Radio Sci.*, *9*(2), 197–203.

Richards, P. G., and D. G. Torr (1988), Ratios of photoelectron to EUV ionization rates for aeronomic studies, *J. Geophys. Res.*, *93*, 4060–4066.

Richards, P. G., J. A. Fennelly, and D. G. Torr (1994), EUVAC: A solar EUV flux model for aeronomic calculations, *J. Geophys. Res.*, *99*, 8981–8992.

Schunk, R. W. (1988), A mathematical model of the middle and high latitude ionosphere, *Pure Appl. Geophys.*, *127*, 255–303.

Sharma, D. K., J. Rai, M. Israil, P. Subrahmanyam, P. Chopra, and S. C. Garg (2004), Enhancement in electron and ion temperatures due to solar flares as measured by SROSS-C2 satellite, *Ann. Geophys.*, *22*, 2047–2052.

Sojka, J. J. (1989), Global scale, physical models of the *F* region ionosphere, *Rev. Geophys.*, *27*, 371–403.

Thome, G. D., and L. S. Wagner (1971), Electron density enhancements in the *E* and F_1 regions of the ionosphere during solar flares, *J. Geophys. Res.*, *76*, 6883–6895.

Tsurutani, B. T., et al. (2005), The October 28, 2003 extreme EUV solar flare and resultant extreme ionospheric effects: Comparison to other Halloween events and the Bastille Day event, *Geophys. Res. Lett.*, *32*, L03S09, doi:10.1029/2004GL021475.

Woods, T., and G. J. Rottman (2002), Solar ultraviolet variability over time periods of aeronomic interest, in *Atmospheres in the Solar System: Comparative Aeronomy*, *Geophys. Monogr. Ser.*, vol. 130, edited by M. Mendillo et al., pp. 221–233, AGU, Washington, D. C.

Woods, T., F. Eparvier, S. Bailey, S. C. Solomon, G. Rottman, G. Lawrence, R. Roble, O. R. White, J. Lean, and W. K. Tobiska (1998), TIMED Solar EUV Experiment, *Proc. SPIE Int. Soc. Opt. Eng.*, *3442*, 180–191.

Woods, T. N., S. M. Bailey, W. K. Peterson, S. C. Solomon, H. P. Warren, F. G. Eparvier, H. Garcia, C. W. Carlson, and J. P. McFadden (2003), Solar extreme ultraviolet variability of the X-class flare on 21 April 2002 and the terrestrial photoelectron response, *Space Weather*, *1*(1), 1001, doi:10.1029/2003SW000010.

Zhang, D. H., Z. Xiao, K. Igarashi, and G. Y. Ma (2002), GPS-derived ionospheric total electron content response to a solar flare that occurred on 14 July 2000, *Radio Sci.*, *37*(5), 1086, doi:10.1029/2001RS002542.

T. Berkey, Physics Department, Utah State University, 4415 Old Main Hill, Logan, UT 84322–4415, USA.

R. W. Schunk, J. J. Sojka, and D. Thompson, Center for Atmospheric and Space Sciences, Utah State University, 4405 Old Main Hill, Logan, UT 84322–4405, USA.

C. G. Smithtro, Air Force Institute of Technology, 2950 Hobson Way, Wright-Patterson AFB, OH 45433–7765, USA. (christopher.smithtro@afit.edu)